

# PHYSICAL REVIEW B

## CONDENSED MATTER

THIRD SERIES, VOLUME 45, NUMBER 12

15 MARCH 1992-II

### Disorder in $\beta''$ -aluminas: Dielectric relaxation and x-ray absorption

M. L. denBoer, Y. S. Pak, K. J. Adamic, and S. G. Greenbaum

*Physics Department, Hunter College, City University of New York, New York, New York 10021*

M. C. Wintersgill

*Physics Department, U.S. Naval Academy, Annapolis, Maryland 21402-5026*

J. F. Lomax

*Chemistry Department, U.S. Naval Academy, Annapolis, Maryland 21402-5026*

J. J. Fontanella

*Physics Department, U.S. Naval Academy, Annapolis, Maryland 21402-5026*

B. Dunn

*Department of Materials Science and Engineering, University of California, Los Angeles, California 90024-1595*

G. C. Farrington

*Department of Materials Science and Engineering, University of Pennsylvania, Philadelphia, Pennsylvania 19104*

(Received 16 October 1991)

$\beta''$ -aluminas substituted with rare-earth elements (Pr, Nd, Er, and Tb) and Sn have been studied using near-edge and extended x-ray-absorption fine structure (NEXAFS and EXAFS). In addition, dielectric-relaxation (DR) measurements have been made on Na- $\beta$ -, Na- $\beta''$ -, and Na-Er- $\beta''$ -alumina. Both the DR and EXAFS results confirm that disorder, particularly in the conduction plane, in the vicinity of the rare-earth ions is a key feature of the  $\beta''$ -aluminas. The NEXAFS studies show that the rare-earth ions are ionized to trivalency and are highly localized; in contrast, Sn is clearly divalent, as in SnO.

### INTRODUCTION

The  $\beta''$ -aluminas are crystalline solid electrolytes consisting of close-packed layers of aluminum and oxygen ions, chemically similar to  $\text{Al}_2\text{O}_3$  separated every 1.13 nm by more open regions containing mobile cations (such as  $\text{Na}^+$ ), often referred to as the conduction planes. The close-packed layers are stabilized by small amounts of  $\text{Mg}^{2+}$ , which substitutes for Al, yielding a typical composition of  $\text{Na}_{1.67}\text{Mg}_{0.67}\text{Al}_{10.33}\text{O}_{17}$  for the parent compound, Na- $\beta''$ -alumina. In addition, the nonstoichiometric incorporation of  $\text{Na}_2\text{O}$  in the material leads to substantial structural disorder in the conduction plane.<sup>1</sup> Related to the high ionic conductivity of the  $\beta''$ -aluminas is the ease with which  $\text{Na}^+$  ions can be replaced by a wide variety of mono-, di-, and trivalent ions.<sup>2,3</sup> Lanthanide-substituted  $\beta''$ -aluminas have been studied recently, with particular emphasis on their optical properties, which include, in some cases, laser activity.<sup>4,5</sup> The observed optical properties depend critically on the local structural and chemi-

cal environment of the rare-earth ion. While the site occupancy of the ions have been investigated by x-ray diffraction,<sup>5</sup> it is clear that conduction-plane disorder is prevalent in the substituted material at least to the same extent as in the parent.

In this paper, we report both dielectric relaxation (DR) and extended x-ray-absorption fine-structure (EXAFS) measurements which attempt to characterize more precisely the specific nature of the conduction-plane disorder, and near-edge x-ray-absorption fine-structure (NEXAFS) measurements to assess the degree of charge localization in the vicinity of the rare-earth ions. In addition to measurements on Er-, Nd-, Pr-, and Tb-substituted  $\beta''$ -aluminas, we present results for divalent Sn-substituted materials.

### EXPERIMENT

Substituted aluminas were made from the parent Na<sup>+</sup>- $\beta''$ -alumina by ion exchange in the appropriate

salt.<sup>6</sup> The completeness of the exchange process was verified through the use of <sup>22</sup>Na tracers. The exchange was approximately 40% for the lanthanide materials and 100% for the material containing tin. These materials are extremely hygroscopic, and precautions were taken to prevent contamination both during preparation and in the measurements.

The temperature dependence of the admittance was measured from about 0.1 to 10 K. The admittance measurements were made at seventeen frequencies between 10 and 10<sup>5</sup> Hz as described previously.<sup>7</sup> Temperatures below 4.2 K were achieved in a dilution refrigerator and the higher-temperature work was done using the same sample holder in the Cryogenics Associates dewar used for previous work.<sup>7</sup> For the Na-β-alumina, a slab approximately 1 mm thick, 5 mm wide, and 15 mm long was cut from a boule for which NMR measurements have been previously reported.<sup>8</sup> This allowed measurements parallel to the conduction planes (perpendicular to the optic axis). As thick samples of Na-β'-alumina were not available, measurements were made on a polycrystalline sample obtained from Ceramtec, Inc. and perpendicular to the conduction planes on a single crystal grown at UCLA. Finally, measurements were carried out perpendicular to the conduction planes on single crystals prepared at UCLA containing both Na and lanthanide ions.

The data were transformed to the complex dielectric constant,  $\epsilon^* = \epsilon' - j\epsilon''$ , using the following procedure. The polycrystalline sample had a regular geometry and was large enough for three terminal measurements to be carried out. From the usual equation for a parallel plate capacitor,

$$C = \epsilon_0 \epsilon' A / d, \quad (1)$$

where  $C$  is the capacitance,  $\epsilon_0$  is the permittivity of free space, and  $A$  and  $d$  are the area and separation of the plates, respectively, it was determined that polycrystalline β' alumina has a value of  $\epsilon'$  of about 13.7 at 1000 Hz and 4.2 K. This was used as the reference value for all samples and the remaining values of  $\epsilon'$  were determined using the approximation that the relative change in  $\epsilon'$  is the same as the relative change in capacitance. Finally, values of  $\epsilon''$  were calculated using the equation

$$\epsilon'' = G\epsilon' / \omega C, \quad (2)$$

where  $G$  is the conductance and  $\omega$  is the angular frequency of the applied electric field.

The x-ray-absorption experiments were carried out on beam line X23B of the National Synchrotron Light Source at Brookhaven National Laboratory, using a separated-crystal Si(111) monochromator with focusing optics to concentrate the light on the small (< 1 mm<sup>2</sup> in area) samples. Measurements were carried out in transmission. The absorption coefficient was taken to be the logarithm of the ratio of the transmitted to the incident flux, as is customary. Due to sample constraints, some measurements were made in the total yield mode, in which the total electron yield is measured as a function of incident photon energy.<sup>9</sup> Standard materials were mea-

sured simultaneously to ensure accurate energy calibration. The spectra shown here have been appropriately calibrated, and are normalized to an increase in absorption of unity at the edge.

## RESULTS AND DISCUSSION

The x-ray-absorption spectrum consists of a series of features extending several hundred electron volts above the absorption edge, as shown by way of example in Fig. 1. This shows the absorption of Pr<sub>4</sub>O<sub>7</sub> in the vicinity of the  $2p_{3/2}$  edge of Pr at about 5940 eV. The sharp features near the edge are the near-edge x-ray-absorption fine structure (NEXAFS). The broad oscillations in the range 50–500 eV above the edge are the well-known extended x-ray-absorption fine structure (EXAFS). In the spectrum of Fig. 1, the  $2p_{1/2}$  edge at about 6410 eV is also apparent.

EXAFS is due primarily to single scattering of the ejected photoelectron from near neighbors of the absorbing atom. Due to the relatively simple processes involved, it is comparatively easy to obtain structural information, including interatomic bond lengths and coordination numbers, from the extended fine structure,<sup>10</sup> at least in materials which are highly ordered on a short-range scale. On the other hand, the near-edge features, due to multiple-scattering processes, are more difficult to relate in a straightforward way to properties of the absorbing material. Facilitating interpretation are the dipole selection rule characteristic of photoabsorption, which constrains the final-state symmetry, and relationship of the edge position to the chemically significant core-level binding energy.

EXAFS analysis proceeds by extracting  $\chi(\mathbf{k})$ , the oscillatory part of the absorption coefficient, weighted by an appropriate power of  $k$ , the wave vector of the outgoing photoelectron. The result is shown in Fig. 2 for Pr<sub>4</sub>O<sub>7</sub> and Pr-β'-alumina. The former compound, used as a reference, is crystalline and the Pr atom is therefore in a

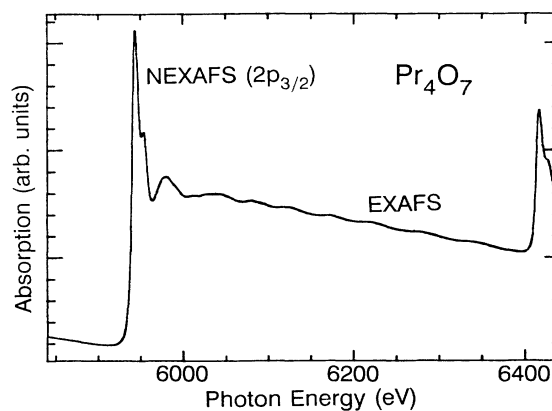


FIG. 1. X-ray-absorption spectrum of PrO<sub>7</sub> in which  $2p_{3/2}$ , ( $L_{III}$ ) and  $2p_{1/2}$  edges are observable. The region extending from about 50 to 500 eV above the absorption edge is the EXAFS region.

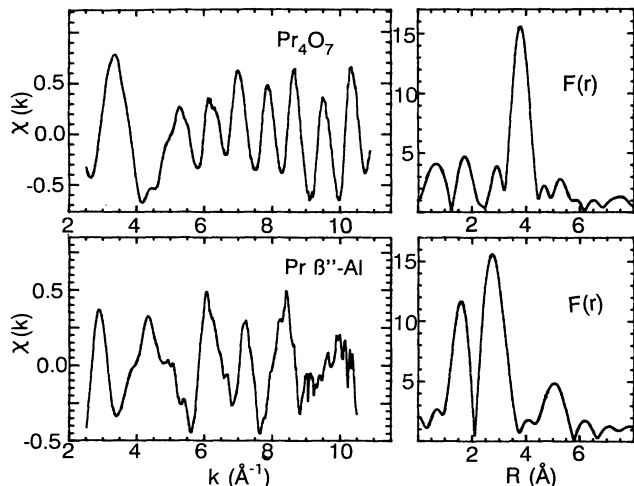


FIG. 2. Weighted EXAFS oscillations of  $\text{Pr}_4\text{O}_7$  and Pr-doped  $\beta''$ -alumina, and corresponding Fourier transforms on the right.

well-ordered local environment. As the EXAFS oscillations are periodic in  $k$ , in this case a Fourier transform exhibits peaks corresponding to interatomic distances, as illustrated in the right panel of Fig. 2. The prominent peak apparent in  $|F(r)|$  for  $\text{Pr}_4\text{O}_7$  represents the Pr-Pr separation in this material. The Pr-O distance is suppressed because O is a weak backscatterer. For Pr- $\beta''$ -alumina, a number of oscillations appear in  $\chi(k)$ ; they are not regular or periodic. This is emphasized in the transform  $|F(r)|$ , in which several weak peaks appear. Calculations show that the position and relative magnitude of these peaks depends on the choice of background, window size, etc., indicating that they do not correspond to physical spacings. Thus the local environment of Pr in Pr- $\beta''$ -alumina, that is the conduction plane, is highly disordered.

Figure 3 shows similar comparisons and results for

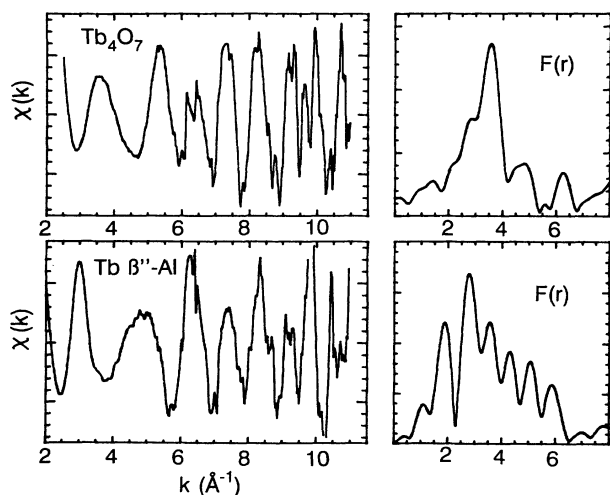


FIG. 3. Weighted EXAFS oscillations of  $\text{Tb}_4\text{O}_7$  and Tb-doped  $\beta''$ -alumina, and corresponding Fourier transforms on the right.

Tb-based compounds. As in the case of  $\text{Pr}_4\text{O}_7$ ,  $\text{Tb}_2\text{O}_3$  exhibits pronounced, regular, features characteristic of an ordered material. On the other hand, the Tb-doped  $\beta''$ -alumina exhibits irregular features with no significant peaks in the transform, indicating that the Tb- $\beta''$ -alumina is also highly disordered, at least in the conduction plane in the vicinity of Tb.

The presence of disorder in the conduction plane is confirmed by the low-temperature dielectric measurements. The temperature dependence of the real and imaginary parts of the dielectric constant are shown in Figs. 4–7 for Na- $\beta$ -alumina and three types of Na- $\beta''$ -alumina. The Na- $\beta$ -alumina was studied both for comparison with previous results in the literature<sup>11,12</sup> and for comparison with  $\beta''$ -alumina for which it appears that no previous low-temperature results have been reported.

As is apparent from Fig. 4(a), the position of the minimum in  $\epsilon'$  at  $10^4$  Hz for Na- $\beta$ -alumina is in good agreement with previous low-temperature audio frequency studies by Anthony and Anderson.<sup>11</sup> As they have pointed out, this behavior is similar to that observed in glasses<sup>13,14</sup> and thus is evidence of disorder. Such behavior is usually interpreted in terms of a two-level tunneling system (TLS). As is clear from Figs. 5(a), 6(a), and 7(a), all of the  $\beta''$ -alumina samples show a minimum in the dielectric constant at low temperatures and thus represent evidence for disorder in those materials also.

Interestingly, the minimum in the curve for Na- $\beta''$ -alumina occurs at a lower temperature than for the Na- $\beta$ -alumina. This shift to lower temperature is indicative of a larger coupling coefficient in the expression for

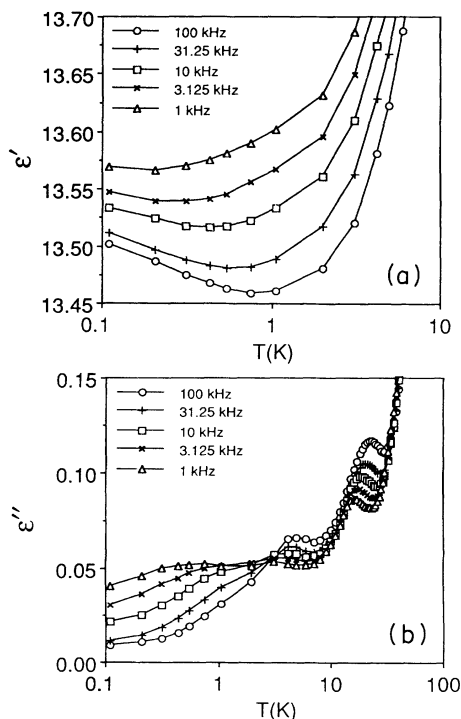


FIG. 4. (a) Real and (b) imaginary parts of the dielectric constant vs temperature for Na- $\beta$ -alumina perpendicular to the optic axis (parallel to the conduction planes).

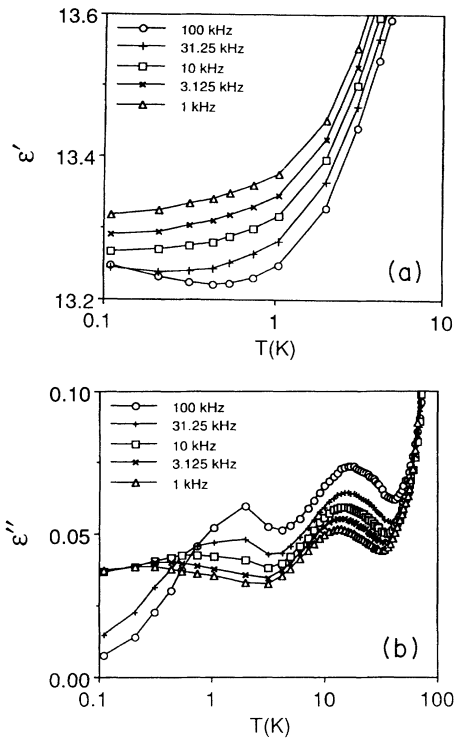


FIG. 5. (a) Real and (b) imaginary parts of the dielectric constant vs temperature for Ceramtec, Inc. Na- $\beta''$ -alumina.

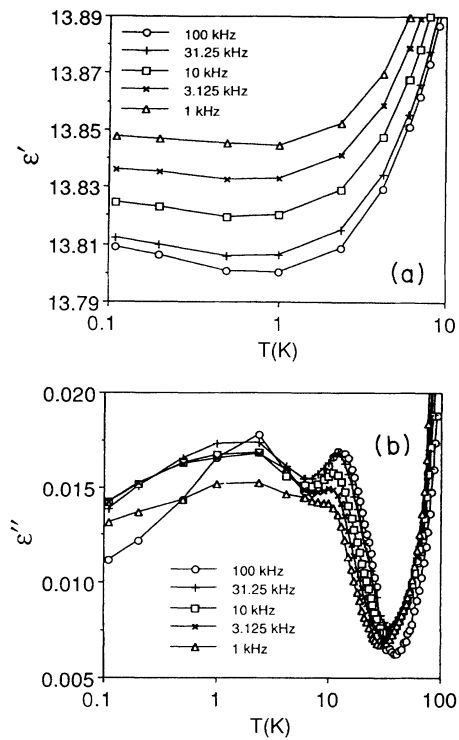


FIG. 7. (a) Real and (b) imaginary parts of the dielectric constant vs temperature for single-crystal Na-Er- $\beta''$ -alumina parallel to the optic axis (perpendicular to the conduction planes).

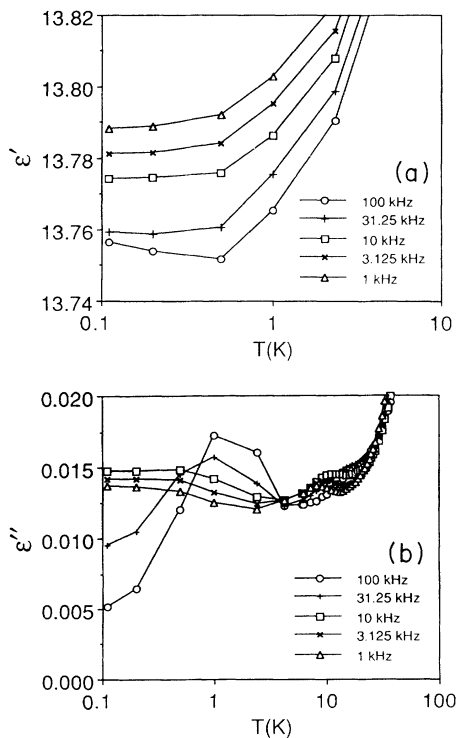


FIG. 6. (a) Real and (b) imaginary parts of the dielectric constant vs temperature for single-crystal Na- $\beta''$ -alumina parallel to the optic axis (perpendicular to the conduction planes).

the TLS relaxation time.<sup>12</sup> This is not surprising since the size of the spinel blocks in  $\beta''$ -alumina is smaller than in  $\beta$ -alumina. Consequently, it might be expected that the separation of the inequivalent wells is smaller in  $\beta''$ -alumina, resulting in a higher tunneling frequency.

On the other hand, it is apparent from Fig. 7(a) for the Na-Er- $\beta''$ -alumina, that the minimum has shifted to a higher temperature than is observed for the pure Na- $\beta''$ -alumina. Consequently, the presence of the erbium ions affects the TLS. Anthony and Anderson have also observed that exchanging monovalent ions affects the TLS.<sup>11</sup> They concluded that the low-energy excitations in  $\beta$ -alumina involve only ions associated with the conducting planes. Since that is the most likely possibility, the present results suggest the same for the  $\beta''$ -aluminas. Consequently, the DR data support the results of the EXAFS studies which indicate that the disorder is primarily in the conduction planes.

It should be pointed out that for both the single-crystal Na- $\beta''$ -alumina and the Na-Er- $\beta''$ -alumina a minimum in the dielectric constant is observed "parallel to the optic axis." It is a very shallow minimum when compared with the data for the polycrystalline material. In fact, Anthony and Anderson<sup>11</sup> were unable to observe a minimum for Na- $\beta$ -alumina parallel to the optic axis. They attributed observed variations with temperature to fringing field effects, i.e., some fraction of the electric field being perpendicular to the optic axis. That may also be the case for the present studies of single-crystal Na- $\beta''$ -

alumina as fringing field effects are significant because of the geometry. Experiments are underway in an attempt to resolve this issue.

Plots of the imaginary part of the dielectric constant as a function of temperature are shown in Figs. 4(b)–7(b). Those results can be compared with previously reported electrical conductivity,  $\sigma$ , data<sup>11,12</sup> since

$$\sigma = \epsilon'' \epsilon_0 \omega, \quad (3)$$

where  $\omega$  is the angular frequency and  $\epsilon_0$  is the permittivity of free space. Consequently, for a given frequency,  $\sigma$  is merely proportional to  $\epsilon''$ . The general form of the curves for the Na- $\beta$ -alumina agrees reasonably well with previously published audio frequency data<sup>11</sup> though the results of the present work are more detailed and show additional features. However, there is a difference between the present data and the previously reported high-frequency results.<sup>12</sup> At the lowest temperatures, the high-frequency conductivity reported in previous work,<sup>12</sup> increases as temperature decreases. The present low-frequency data, which are similar to the previous audio frequency results,<sup>11</sup> show decreasing conductivity with decreasing temperature. This difference is attributed to the difference in frequency and temperature ranges over which the data are taken.

It is apparent from Figs. 4(b)–7(b) that two loss peaks are observed below 30 K for all samples. This is reminiscent of  $\tan\delta$  data (which is again approximately proportional to  $\epsilon''$  because  $\tan\delta = \epsilon''/\epsilon'$ ) for fused silica containing 1200 ppm of OH where a peak is found below 1 K and another is found at about 20 K.<sup>15</sup> In the case of the fused silica,  $\epsilon''$  approaches zero above the second peak whereas in the present case the loss continues to increase as temperature increases.<sup>11</sup> The increasing loss in the case of the  $\beta$ - and  $\beta'$ -aluminas is attributable to the ionic conductivity. The similarity between dielectric loss data for the various  $\beta$ - and  $\beta'$ -aluminas and fused silica containing hydroxyl ions once again confirms the existence of disorder in the  $\beta$ - and  $\beta'$ -aluminas, presumably in the conduction planes.

Additional information about the local electronic structure is available from the fine structure near the x-ray-absorption edge (NEXAFS). As mentioned, this structure is difficult to analyze quantitatively; we therefore proceed by comparison with standards. In Fig. 8(a), we compare the  $2p_{3/2}$  ( $L_{III}$ ) edge for  $\text{Pr}_4\text{O}_{11}$  to that of Pr- $\beta'$ -alumina. The prominent peak or "white line" in this spectrum is due to dipole-allowed transitions into unoccupied final states of  $d$  symmetry (the Pr  $5d$  band, in this case). This feature is even more prominent and sharper in the alumina than in the oxide. There is no evidence of a second feature, as would be the case as seen in the mixed valent  $\text{Pr}_4\text{O}_{11}$ . In the simplest interpretation, the peak amplitude reflects a higher density of empty  $d$  states in the vicinity of the absorbing Pr ion in the oxide. The sharpness, which is characteristic of isolated-atom absorption, indicates that these states are highly localized, unhybridized by interaction with the states of nearby ligands. We conclude that the Pr is in a localized, almost atomiclike, trivalent state. This localization may

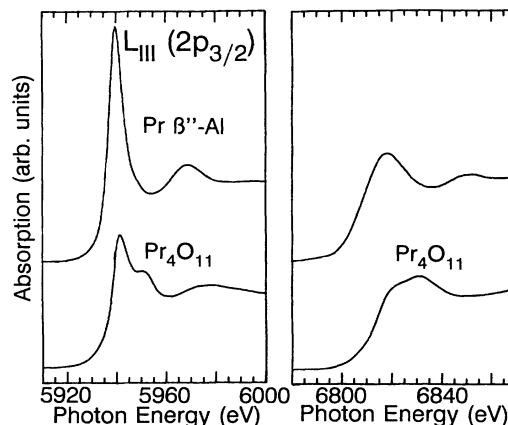


FIG. 8. (a)  $2p_{3/2}$  ( $L_{III}$ ) and (b)  $2s$  ( $L_I$ ) absorption edges of  $\text{Pr}_4\text{O}_{11}$  and Pr-substituted  $\beta'$ -alumina.

account for the optical-absorption characteristics generally observed in the lanthanide  $\beta'$ -aluminas.<sup>4</sup> In particular, localization coupled with the large cation separation deduced from x-ray-diffraction measurements<sup>5</sup> may also be an important factor in the long fluorescence lifetimes of these materials.<sup>4</sup>

On the other hand, the  $2s$  ( $L_I$ ) spectrum of  $\text{Pr}_4\text{O}_{11}$  and Pr- $\beta'$ -alumina shown in Fig. 8(b) is remarkably different from the  $2p$ ; no prominent peak is present. This is expected because, for the  $2s$  level, dipole-allowed transitions are to empty  $p$  states, which, in trivalent Pr, are much less localized and have a much lower partial density of states.

Similar results are obtained from the near-edge spectra of  $\text{NdF}_3$  and Nd- $\beta'$ -alumina, compared in Figs. 9(a) and 9(b).  $\text{NdF}_3$  is more purely ionic than the corresponding oxide; accordingly, the  $2p_{3/2}$  peak is sharper and more prominent than in  $\text{Pr}_4\text{O}_{11}$ . Nevertheless, the Nd- $\beta'$ -alumina  $2p_{3/2}$  spectrum exhibits a still sharper and more prominent peak. This indicates that the rare-earth element in the alumina is highly ionic, oxidized to trivalency by complete removal of three electrons, and remains as

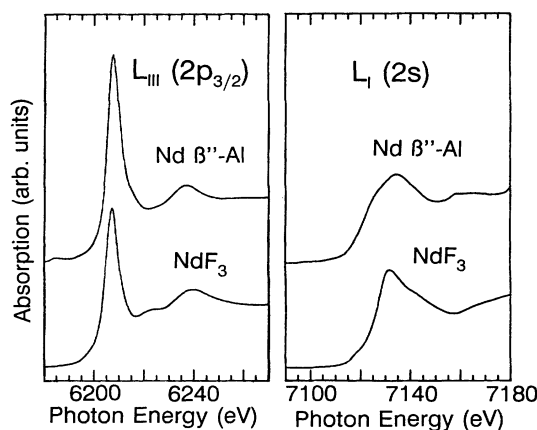


FIG. 9. (a)  $2p_{3/2}$  ( $L_{III}$ ) and (b)  $2s$  ( $L_I$ ) absorption edges of  $\text{NdF}_3$  and Nd-substituted  $\beta'$ -alumina.

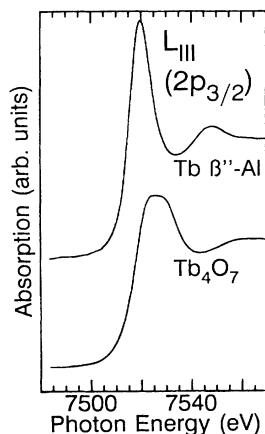


FIG. 10.  $2p_{3/2}$  ( $L_{III}$ ) absorption edge of  $Tb_4O_7$ - and Tb-substituted  $\beta''$ -alumina.

an essentially isolated ion in the alumina matrix. Once again, the  $2s$  spectrum of these materials, which probe unoccupied  $p$  states, do not show effects due to the high local density of  $d$  states.

In Fig. 10 we compare the  $2p_{3/2}$  spectrum for  $Tb_4O_7$  to that for Tb- $\beta''$ -alumina. The alumina has a much sharper and larger white-line feature, reflecting, as for other rare-earth elements, the large localized density of unoccupied  $d$  states in this material. The highly ionic nature of lanthanide ions in  $\beta''$ -alumina has also been inferred from site-selective spectroscopic measurements of Eu(III)-substituted  $\beta''$ -alumina.<sup>16</sup>

Finally, we compare in Figs. 11(a) and 11(b) the  $L$ -shell spectra of Sn compounds,  $SnO_2$ ,  $SnO$ , and Sn- $\beta''$ -alumina. The valence band of Sn is an  $sp$  hybrid, so that oxidized Sn has a high density of unoccupied  $p$  states. These are inaccessible via a dipole transition from an initial  $p$  state. Therefore, no prominent peak is visible at the  $2p_{3/2}$  edge in any of these materials, while a very large peak is apparent at the  $2s$  edge which can directly fill these states. This is the opposite of the situation for the rare-earth elements, and is a direct consequence of the different final-state symmetry. A number of small, sharp peaks are observed for  $SnO_2$ , and to a lesser extent for  $SnO$ . While no detailed calculations of the near-edge structure are available for these materials, these peaks indicate effects due to ionicity and crystal-field splitting. The effects are weaker and broader in the alumina, presumably due to the absence of crystal-field splitting, reflecting either a highly symmetric site or, more likely, effective angular averaging due to random disorder. The  $2s$  peaks in the alumina is much smaller than in the oxides, probably a consequence of the lower density of unoccupied states in the alumina. This is also different from the rare-earth elements, which, as noted, are

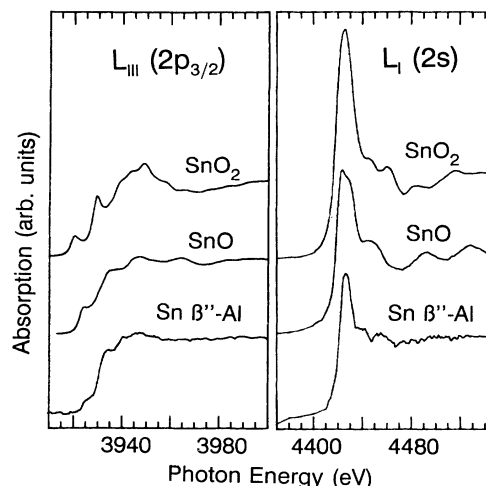


FIG. 11. (a)  $2p_{3/2}$  ( $L_{III}$ ); and (b)  $2s$  ( $L_1$ ) absorption edges of  $SnO_2$ -,  $SnO$ -, and Sn-substituted  $\beta''$ -alumina.

characterized by a high density of very localized  $d$  states. The  $p$  states are more extended. Although the alumina spectrum is not exactly like either oxide, it is much closer to  $SnO$ , indicating that the Sn ions in Sn- $\beta''$ -alumina are predominantly divalent, as in  $SnO$ , and are clearly not tetravalent as in  $SnO_2$ . This is also different from the rare-earth case.

## CONCLUSIONS

Disorder is a key feature of the rare-earth-substituted  $\beta''$ -aluminas, as evidenced by both dielectric relaxation and EXAFS results. Both experiments indicate that this disorder is primarily in the conduction plane.

NEXAFS results indicate that substituted rare-earth ions are ionized to trivalency and are highly localized. This is demonstrated dramatically for the case of Nd-substituted  $\beta''$ -alumina, which exhibits a sharper absorption edge than  $NdF_3$  standards. The localized electronic nature of the rare-earth ions is largely responsible for the optical properties of the doped  $\beta''$ -aluminas. Finally, Sn-substituted  $\beta''$ -alumina is predominantly divalent, as in  $SnO$ , and is clearly not oxidized to tetravalency, as in  $SnO_2$ .

## ACKNOWLEDGMENTS

The portion of the work at Hunter College of CUNY was supported in part by PSC-CUNY. The work of M.C.W. and J.F.L. was supported in part by the National Science Foundation and the Naval Academy Research Council. Two of us (B.D. and G.C.F.) acknowledge support from the Office of Naval Research.

- <sup>1</sup>M. Bettman and C. R. Peters, *J. Phys. Chem.* **73**, 1774 (1969);  
B. Dunn and G. C. Farrington, *Solid State Ion.* **18&19**, 31 (1986).
- <sup>2</sup>J. L. Briant and G. C. Farrington, *Solid State Chem.* **33**, 385 (1980).
- <sup>3</sup>G. C. Farrington and B. Dunn, *Solid State Ion.* **7**, 267 (1982).
- <sup>4</sup>M. Jansen, A. Alfrey, O. M. Stafsud, B. Dunn, D. L. Yang, and G. C. Farrington, *Opt. Lett.* **9**, 119 (1984).
- <sup>5</sup>W. Carrillo-Cabrera, J. O. Thomas, and G. C. Farrington, *Solid State Ion.* **28-30**, 317 (1988).
- <sup>6</sup>S. Sattar, B. Ghosal, M. L. Underwood, H. Mertway, M. A. Saltzberg, W. S. Frydrych, G. S. Rohrer, and G. C. Farrington, *J. Solid State Chem.* **196**, 231 (1986).
- <sup>7</sup>C. G. Andeen, D. Link, and J. J. Fontanella, *Phys. Rev. B* **16**, 3762 (1977).
- <sup>8</sup>S. G. Greenbaum, U. Strom, and M. Rubenstein, *Phys. Rev. B* **26**, 5226 (1982).
- <sup>9</sup>T. Guo and M. L. denBoer, *Phys. Rev. B* **31**, 6233 (1985).
- <sup>10</sup>P. A. Lee, P. H. Citrin, P. Wisenberger, and B. N. Kincaid, *Rev. Mod. Phys.* **53**, 769 (1981).
- <sup>11</sup>P. J. Anthony and A. C. Anderson, *Phys. Rev. B* **19**, 5310 (1979).
- <sup>12</sup>U. Strom, M. von Schickfus, and S. Huncklinger, *Phys. Rev. B* **25**, 2405 (1982).
- <sup>13</sup>G. Frossati, J. le G. Gilchrist, J. C. Lasjaunias, and W. Meyer, *J. Phys. C* **10**, L515 (1977).
- <sup>14</sup>M. von Schickfus and S. Huncklinger, *J. Phys. C* **9**, L439 (1976).
- <sup>15</sup>W. A. Phillips, *Philos. Mag.* **43**, 747 (1981).
- <sup>16</sup>M. Saltzberg and G. C. Farrington, *J. Solid State Chem.* **83**, 272 (1989).